J. Fluid Mech. (2022), *vol*. 943, A49, doi:10.1017/jfm.2022.443

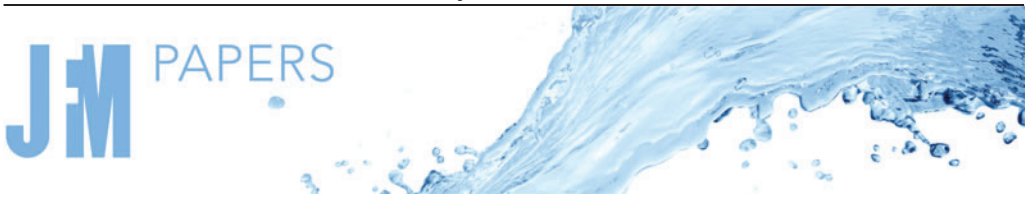

A physics-based model for wind turbine wake expansion in the atmospheric boundary layer

Dara Vahidi[1] **and Fernando Porté-Agel**[1],†

[1]École Polytechnique Fédérale de Lausanne (EPFL), Wind Engineering and Renewable Energy Laboratory (WiRE), EPFL-ENAC-IIE-WIRE, CH-1015 Lausanne, Switzerland

(Received 7 December 2021; revised 27 April 2022; accepted 12 May 2022)

Analytical wind turbine wake models are widely used to predict the wake velocity deficit. In these models, the wake growth rate is a key parameter specified mainly with empirical formulations. In this study, a new physics-based model is proposed and validated to predict the wake expansion downstream of a turbine based on the incoming ambient turbulence and turbine operating conditions. The new model utilises Taylor diffusion theory, the Gaussian wake model, turbulent mixing layer theory and the analogy between wind turbine wake expansion and scalar diffusion. These components ensure that the model conserves mass and momentum in the far wake and accounts for the ambient turbulence and turbine-induced turbulence effects on the wake expansion. To account for the turbulence relevant scales that contribute to the wake expansion, the model uses the root-mean-square of the low-pass filtered radial velocity component. A simplified version that only requires the unfiltered velocity standard deviation and turbulence integral scale is also proposed. In addition, a new relation for the near-wake length is derived. The model performance is validated using large-eddy simulation data of a wind turbine wake under neutral atmospheric conditions with a wide range of incoming turbulence levels. The results show that the proposed model yields reasonable predictions of the wake width, maximum velocity deficit and near-wake length. In the case with a relatively low incoming streamwise turbulence intensity of 0.05, the ambient and turbine-induced terms in the model contribute almost equally to the wake width, rendering them both crucial for reasonable wake predictions.

Key words: wakes, turbulent boundary layers

† Email address for correspondence: fernando.porte-agel@epfl.ch

1. Introduction

Wind energy offers significant potential for short-term and long-term reduction of greenhouse gas emissions (Edenhofer *et al.* 2011). In order to make use of this potential and reduce the usage of unsustainable fossil fuels, wind power production and the size of wind farms continue to grow worldwide. In wind farms, many of the wind turbines are operating in the wakes of upstream turbines. Thus, they are exposed to lower incoming wind velocities than those operating under undisturbed conditions. As a result, the inevitable wake interactions are responsible for significant power losses in wind farms (Sanderse, Van der Pijl & Koren 2011; Porté-Agel, Bastankhah & Shamsoddin 2020). Moreover, the wake flow contains the accumulated turbulence from the atmosphere and upstream turbines (Frandsen 2007; Stevens & Meneveau 2017), which can impose serious structural and fatigue loads on the downstream turbines. To have a prediction of the wake flow for applications such as wind farm layout optimisation, analytical wake models, as simple and computationally efficient tools, are widely used in the wind energy community (Duckworth & Barthelmie 2008; Göçmen *et al.* 2016; Porté-Agel *et al.* 2020). Despite being less accurate than high-fidelity numerical simulations, analytical models have the added value of providing fundamental insight into the physics, as their derivation relies on the basic equations governing the conservation of flow properties (Porté-Agel *et al.* 2020). The following subsection provides a brief overview of the existing analytical wake models.

1.1. *Review of existing analytical wake models*

There exist many studies focused on developing analytical wind turbine wake models. In one of the pioneering studies, Jensen (1983) proposed an analytical wake model that assumes a top-hat shape for the velocity deficit and a linear wake growth rate (k_t), with values of 0.04–0.05 for offshore and 0.075 for onshore turbines (Barthelmie *et al.* 2009; Göçmen *et al.* 2016). Despite being very popular in the literature and commercial software such as WAsP, WindPRO, WindSim and OpenWind, the Jensen model underestimates the velocity deficit due to the assumption of a top-hat profile and the fact that its derivation is only based on mass conservation (Bastankhah & Porté-Agel 2014). Frandsen *et al.* (2006), based on mass and momentum conservation in a control volume around the turbine, derived the following relation for the normalised wake velocity deficit, assuming a top-hat profile:

$$\frac{\Delta U(x)}{U_\infty} = \frac{1}{2}\left(1 - \sqrt{1 - \frac{2C_T}{\beta_F + \alpha_F x/d}}\right), \tag{1.1}$$

where U_∞ is the mean incoming wind speed, C_T is the turbine thrust coefficient, d is the rotor diameter and $\Delta U(x) = U_\infty - U_w(x)$, in which $U_w(x)$ is the wake velocity in the streamwise direction. In this model, the expansion factor (α_F) is of the order of $10k_t$ and β_F is defined as the ratio of the cross-sectional area of the wake after the initial wake expansion to the area swept by the wind turbine blades, and is a function of C_T ($\beta_F = \frac{1}{2}(1 + \sqrt{1 - C_T})/\sqrt{1 - C_T}$; a detailed derivation was provided by Frandsen *et al.* 2006). The assumption of a top-hat profile for the wake velocity deficit profiles can lead to substantial errors (underestimation of the velocity deficit at the wake centre and overestimation at the wake edges) in wind farm power predictions (Bastankhah & Porté-Agel 2014). Based on different numerical and experimental data (Chamorro & Porté-Agel 2009; Wu & Porté-Agel 2012), a self-similar Gaussian distribution can provide an acceptable representation of the wake velocity deficit in the far wake. Following this observation and based on mass and momentum conservation, Bastankhah & Porté-Agel

(2014) proposed a Gaussian model for the normalised velocity deficit profiles:

$$\frac{\Delta U(x)}{U_\infty} = \left(1 - \sqrt{1 - \frac{C_T}{8(\sigma(x)/d)^2}}\right) \times \exp\left(-\frac{r^2}{2\sigma(x)^2}\right), \tag{1.2}$$

where $\sigma(x)$ is the wake width and assumed to grow linearly ($\sigma(x) = k^*(x - x_{NW}) + d/\sqrt{8}$) with a wake growth rate of k^* and the wake width of $d/\sqrt{8}$ at the end of the near wake (x_{NW}). In order to use the Gaussian model, an estimation of k^* is required based on the incoming flow turbulence characteristics (Wu & Porté-Agel 2012; Abkar & Porté-Agel 2015). To close the model, Niayifar & Porté-Agel (2016) proposed an empirical linear relation between the wake growth rate and the streamwise turbulence intensity (I_u) ($k^* = 0.38I_u + 0.004$), based on large-eddy simulation (LES) results of wind turbine wakes under neutral atmospheric conditions. It should be noted that this relation was derived for a specific range of streamwise turbulence intensity ($0.06 < I_u < 0.15$) and for $C_T \approx 0.8$. From field measurements, Carbajo Fuertes, Markfort & Porté-Agel (2018) and Brugger *et al.* (2019) derived a similar empirical linear relation for the wake growth rate as a function of streamwise turbulence intensity, with a slope varying between 0.3 and 0.35. More recently, Teng & Markfort (2020) proposed a calibration procedure for modelling wind farm wakes using a simple analytical approach and wind turbine operational data obtained from the Supervisory Control and Data Acquisition (SCADA) system. As part of this procedure, they derived an empirical linear relation for the wake growth rate as a function of streamwise turbulence intensity with a slope of 0.26.

Several studies focused on the similarities between the transport of a passive scalar in the atmosphere and momentum transport in wind turbine wakes. The dominant role of large-scale atmospheric turbulence and the contribution of the lateral and vertical velocity fluctuations to the transport are the basis of these similarities. In the dynamic wake meandering model (Larsen *et al.* 2008), it is assumed that the velocity deficit in the wake is transported similarly to a passive scalar in the atmospheric boundary layer (ABL). Following the same analogy and based on Taylor diffusion theory (Taylor 1922), Cheng & Porté-Agel (2018) proposed a model for the wind turbine wake width in a turbulent boundary layer:

$$\sigma_{wake,y} = \sqrt{Sc_t}\langle v^2_{(T'/\beta)}\rangle^{1/2} T', \tag{1.3}$$

where $\sigma_{wake,y}$ represents the wake width in the lateral direction, Sc_t is the turbulent Schmidt number (Reynolds 1976), β is the Lagrangian to Eulerian scale factor (defined in § 2.1.1), $\langle v^2_{(T'/\beta)}\rangle^{1/2}$ is the root-mean-square of the lateral velocity component filtered in time using a filter of size T'/β and T' is the travel time with respect to the virtual origin proposed in the model (a detailed schematic is provided in Cheng & Porté-Agel 2018, p. 4). The model can provide reasonable predictions for the wake width in the presence of high atmospheric turbulence. However, an underestimation of the wake width by the model is found compared with that obtained from LES data in the case of low ambient turbulence due to the non-negligible contribution of the turbine-induced turbulence to the wake growth rate.

Based on numerical and experimental observations (Xie & Archer 2015; Carbajo Fuertes *et al.* 2018), the far-wake velocity deficit profiles show a self-similar Gaussian behaviour. In contrast, the near-wake velocity deficit profiles are strongly affected by the turbine characteristics (blade and nacelle geometries) and, therefore, show a less universal behaviour (Bastankhah & Porté-Agel 2016). In order to model the wake velocity deficit distribution in the near wake and far wake with a single function, several studies proposed

the use of shape functions such as double-Gaussian (Keane *et al.* 2016; Schreiber, Balbaa & Bottasso 2020*a*; Keane 2021) or super-Gaussian (Shapiro *et al.* 2019; Blondel & Cathelain 2020) for the wake velocity deficit profile. In the model presented by Shapiro *et al.* (2019), the wake diameter (d_w) is assumed to expand linearly ($d_w(x) = 1 + 2k_w x/d$) with an expansion coefficient of $k_w = \alpha u_*/U_\infty$. In this model, the wake expansion rate is a function of the atmospheric shear velocity (u_*) and α is a tunable parameter based on the operating condition. The proposed super-Gaussian wake profile is of the form

$$\Delta U(x,t) = \delta u_n(x,t) C_f(x) \exp\left(-\frac{d^2}{8\sigma_0^2}\left(\frac{2r}{d_w(x)d}\right)^{p(x)}\right), \tag{1.4}$$

in which $\delta u_n(x,t)$ is the spatiotemporal evolution of the wake velocity deficit at each downwind location, $\sigma_0 = d/4$, $p(x)$ is the smoothness parameter and $C_f(x)$ is the scaling factor calculated from mass conservation. Based on the evolution of the smoothness parameter, (1.4) transitions between a top-hat profile in the near wake to a Gaussian distribution in the far wake. In another model and to predict more details of the near-wake flow, a double-Gaussian shape function was proposed to resemble more closely the near-wake velocity deficit profile (including the nacelle effect) and transition to a Gaussian profile in the far wake (Keane *et al.* 2016; Schreiber *et al.* 2020*a*). In their derivations, these models follow closely the Gaussian wake model (Bastankhah & Porté-Agel 2014) in the far wake but with more case-specific parameters tunable based on the operating conditions.

1.2. *Motivation of the study*

It is important to highlight that many of the aforementioned models require the specification of the wake growth rate parameter as the main input. This parameter depends on many factors, including the incoming flow turbulence characteristics (e.g. turbulence intensity) and turbine operating conditions. Currently, the wake growth rate is either taken as a constant (Jensen 1983) or calculated from empirical linear relation as a function of the streamwise turbulence intensity (Niayifar & Porté-Agel 2016; Brugger *et al.* 2019; Teng & Markfort 2020). More recently, Schreiber *et al.* (2020*b*) introduced a method to improve the performance of the wake engineering models to predict wind farm flows by learning the associated parameters (including the wake growth rate) of the baseline model from operational data. Alongside these data-driven approaches, the importance of having a robust estimation of the wake model parameters was discussed by Howland *et al.* (2020) in the context of optimal closed-loop wake steering approaches. Therefore, accurate modelling of the wake growth rate is of great importance to the wind energy community. In this paper, we aim to develop a physics-based model for wind turbine wake growth rate, which takes into account the effects of the incoming turbulence level and turbine operating conditions. The proposed model is based on Taylor diffusion theory, the Gaussian wake model (to conserve mass and momentum in the far wake), turbulent mixing layer self-similarity and the analogy of wind turbine wake expansion and scalar diffusion from a disk source. As an integral part of the model, a new relation for the near-wake length is derived as a function of the ambient turbulence level and turbine operating conditions. In order to examine the performance of the proposed model, the results are validated against LES data of a real-scale model wind turbine wake under neutral ABL conditions with different incoming turbulence intensity levels.

This paper is structured as follows. In § 2, a brief description of the model components is given, followed by the model derivation. In § 3, the performance of the model is assessed using LES data. The concluding remarks are presented in § 4. Finally, within

Appendix A, the reader may find a step-by-step summary of the model as presented in § 2. This summary includes the required inputs, the outputs, a step-by-step procedure of model implementation along with the nomenclature of key variables.

2. Wake model

2.1. *Model components*

2.1.1. *Taylor diffusion theory*

Taylor diffusion theory was proposed as a model for the mean square of the lateral distribution of a large number of particles, σ_y^2, behind a point source in a field of stationary and homogeneous turbulence (Taylor 1922):

$$\frac{1}{2}\frac{\mathrm{d}}{\mathrm{d}t}\sigma_y^2 = \sigma_v^2 \int_0^t R_\zeta \,\mathrm{d}\zeta, \tag{2.1}$$

where σ_v is the standard deviation of the lateral velocity component and R_ζ represents the auto-correlation function (ACF) of the lateral velocity component. According to (2.1), the rate of change of σ_y with time is a decreasing function of travel time for continuous plumes (Hanna, Briggs & Hosker 1982). Therefore, the contribution of the small scales to the plume growth decreases as the plume spreads. Instead, much of the diffusion is associated with eddies with diameters roughly equal to and larger than σ_y (a detailed proof is provided by Pasquill & Smith 1983). As described and implemented by Cheng & Porté-Agel (2018), this effect can be modelled by applying a low-pass filter on the velocity time series. In addition, Gifford (1955) and Hay & Pasquill (1959) suggested that the Lagrangian and Eulerian spectra are similar in shape but different in scale. The scale factor (β) can be formally defined as the ratio of the Lagrangian to the Eulerian time scales, and it is inversely proportional to the turbulence intensity. This is consistent with the experimental results of Hanna (1981) who found that, in the daytime ABL,

$$\beta = \frac{T_L}{T_E} \approx \frac{0.7}{I_{v(w)}}, \tag{2.2}$$

where T_L and T_E are the Lagrangian and Eulerian integral time scales, respectively, and $I_{v(w)}$ is the lateral (vertical) turbulence intensity. By introducing proper velocity, length and time scales, one can rewrite (2.1) as a spreading problem with a time-dependent diffusivity:

$$\frac{1}{2}\frac{\mathrm{d}}{\mathrm{d}t}\sigma_y^2 = K_T(t), \tag{2.3}$$

where K_T represents the turbulent diffusivity. Equation (2.3) is the core of the new analytical model. This approach has been used by several studies (Eames *et al.* 2011; Eames, Jonsson & Johnson 2011*b*) to analyse the ambient turbulence contribution to the evolution of the wake velocity deficit of different geometries such as spheres and cylinders.

2.1.2. *Turbulent mixing layer*

Due to the difference in the velocity between the region downstream of the rotor and the undisturbed incoming flow, a cylindrical shear layer forms at the wake edge in the region downstream of the rotor. The expansion of this layer while traveling downstream is considered as one of the sources of the wake velocity distribution and the generated turbulence in the wake (Crespo, Hernandez & Frandsen 1999). As described by Pope (2000), the mixing layer is the turbulent flow that forms between

two uniform nearly parallel streams of different velocities U_l and U_h. The flow depends on the non-dimensional parameter U_l/U_h and two characteristic velocities defined as $U_c = (U_h + U_l)/2$ and $U_s = U_h - U_l$ referred to as the convective and shear velocity, respectively. In addition, an error function profile can be used to model the velocity distribution of this type of flow (Pope 2000):

$$U = U_c + \frac{U_s}{2}\mathrm{erf}\left(\frac{\xi}{\sigma_e\sqrt{2}}\right), \tag{2.4}$$

where σ_e is the mixing layer characteristic length and ξ corresponds to the cross-stream coordinate in the plane of interest. As derived theoretically (from the flow self-similarity) and also shown experimentally and numerically (Brown & Roshko 1974; Dimotakis 1986; Pope 2000), a mixing layer grows linearly with the downstream distance. If the characteristic length scale is defined as σ_e in (2.4), one can define the spreading parameter as follows:

$$S' = \frac{U_c}{U_s}\frac{\mathrm{d}\sigma_e}{\mathrm{d}x} = \frac{1}{U_s}\frac{\mathrm{d}\sigma_e}{\mathrm{d}t}, \tag{2.5}$$

which has been shown experimentally and numerically to be constant and within the range of 0.023–0.043 (Dimotakis 1986; Pope 2000). In the context of the new model for wind turbine wake expansion, (2.5) will be used to include the effect of the turbine-induced turbulence on the wake expansion, as explained in § 2.2 and summarised in Appendix A.

2.1.3. *Scalar diffusion from a disk source*

As discussed previously, there exist similarities between the transport of a passive scalar in the atmosphere and momentum transport in wind turbine wakes (Larsen *et al.* 2008; Cheng & Porté-Agel 2018). Based on these similarities, the focus of this study is on the analogy between the wind turbine wake expansion and the scalar diffusion from a continuous disk source (Crank 1979). In this case, the diffusing substance is initially distributed uniformly in a disk with a radius of R and left to diffuse throughout the surrounding medium. By assuming a constant diffusion coefficient D_c (Crank 1979, p. 28), the following relation defines the distribution of the scalar with time:

$$C(r,t) = \int_0^t \left(\frac{C_0}{2D_c t}\exp\left(\frac{-r^2}{4D_c t}\right)\int_0^R \exp\left(\frac{-r'^2}{4D_c t}\right) I_0\left(\frac{rr'}{2D_c t}\right) r'\,\mathrm{d}r'\right)\mathrm{d}t, \tag{2.6}$$

where C_0 is the initial concentration, I_0 is the modified Bessel function of the first kind of order zero and r is the radial coordinate. The integral in (2.6) does not have an analytical solution, except on the axis $r = 0$, where (2.6) becomes

$$C(0,t) = C_0\left(1 - \exp\left(\frac{-R^2}{4D_c t}\right)\right). \tag{2.7}$$

Figure 1(*a*) shows the numerical solution of (2.6) for different values of the normalised scalar mixing layer characteristic length ($\sigma_e/D = \sqrt{2tD_c}/D$, characteristic length of the error function solution of a planar mixing layer) with D the source diameter, while figure 1(*b*) shows the analytical solution of the maximum concentration in the centreline given by (2.7). From figure 1(*a*), it is clear that the concentration profile evolves from the initial top-hat shape to a Gaussian shape, which is similar to the behaviour of the velocity deficit profile in a wind turbine wake with increasing travel time and, thus, streamwise distance (Shapiro *et al.* 2019). It is important to note that the normalised solution presented

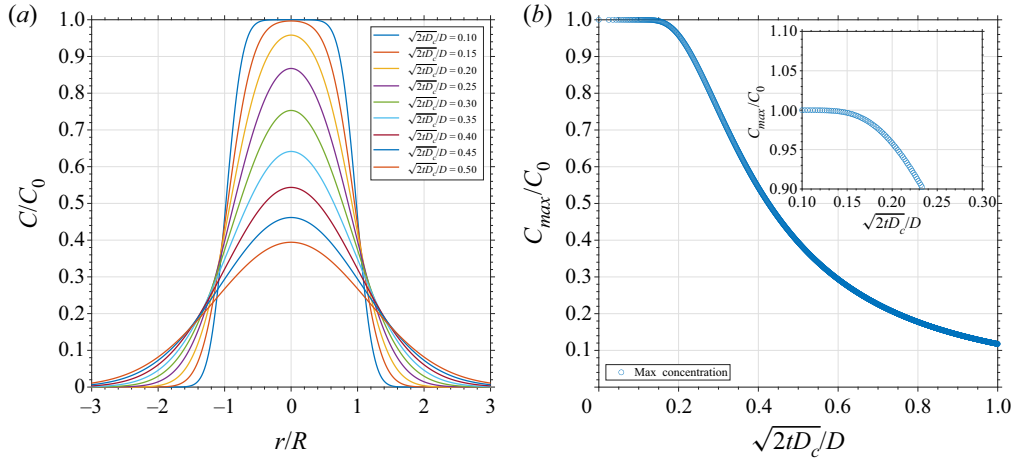

Figure 1. Concentration distribution for a disk source. (*a*) Gradual transformation of the concentration profile from a top-hat profile to a Gaussian distribution. (*b*) Maximum concentration on the centreline as a function of normalised scalar mixing layer characteristic length $\sqrt{2tD_c}/D$.

in figure 1(*a*) is unique for any given σ_e/D. In order to understand when and how well the solution of (2.6) given in figure 1(*a*) can be approximated by a Gaussian profile, a Gaussian distribution is fitted to each profile, and the standard deviation of the fitted Gaussian curve (σ_{wake}) and the correlation coefficient (R^2) of the corresponding fit are calculated. Figure 2(*a*) shows the R^2 of the Gaussian fit as a function of σ_e/D. From this figure, it is clear that a value of $R^2 = 0.99$, often used as a threshold to determine the beginning of the Gaussian behaviour characteristic of the far wake (Sørensen *et al.* 2015; Carbajo Fuertes *et al.* 2018), is achieved for $\sigma_e/D \approx 0.18$. This result will be used in § 2.3 in the context of the new model to derive the near-wake length. Figure 2(*b*) shows the value of σ_{wake}/σ_e as a function of σ_e/D obtained from the numerical solution of (2.6), together with the curve fit. The proposed fit provides a simple equation (within a 99.9 % confidence) for the relationship between σ_e and σ_{wake}:

$$\frac{\sigma_{wake}}{\sigma_e} = 1.95\exp\left(-6.19\frac{\sigma_e}{D}\right) + 10.96\exp\left(-20.05\frac{\sigma_e}{D}\right) + 1.03. \tag{2.8}$$

In the context of the proposed analytical model for wake expansion, (2.8) will be used to compute the wake width (σ_{wake}) in the far wake from the mixing layer characteristic length (σ_e) computed using the expression derived in the next section using Taylor diffusion theory. A summary of the final model framework, including how (2.8) is used, is provided in Appendix A.

2.2. *Model derivation*

We start with Taylor diffusion theory and rewrite the spreading equation for a mixing layer based on the turbulent diffusivity:

$$\frac{1}{2}\frac{\mathrm{d}}{\mathrm{d}t}\sigma_{ey}^2 = K_T(t), \tag{2.9}$$

where σ_{ey} represents the lateral characteristic length of a mixing layer. Based on the similarity of a passive scalar transport in the atmosphere and momentum transport in wind turbine wakes, the wake model can be constructed based on (2.9) with an equivalent

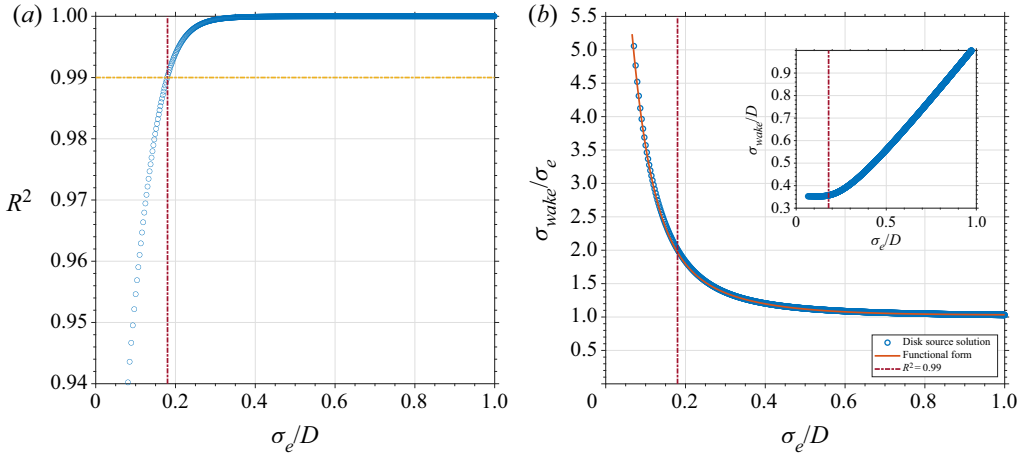

Figure 2. (*a*) Gaussian fit R^2 and (*b*) the ratio of Gaussian fit standard deviation to mixing layer characteristic length as a function of non-dimensional mixing layer length scale calculated from disk source analogy. The vertical lines corresponds to $\sigma_e/D = 0.18$ which results in $R^2 \approx 0.99$. D is the source diameter.

turbulent viscosity (ν_T). Here, we assume two main factors contribute to the wind turbine wake growth: the ambient turbulence and the turbine-induced turbulence. As proposed by Lissaman (1979) and Ainslie (1988), one possibility is to add up the effect of the ambient and turbine-induced turbulence in the equivalent turbulent viscosity. Hence, (2.9) can be written in the following form:

$$\frac{1}{2}\frac{\mathrm{d}}{\mathrm{d}t}\sigma_{ey}^2 = \sigma_{ey}\frac{\mathrm{d}\sigma_{ey}}{\mathrm{d}t} = \nu_{Tamb} + \nu_{Tshear}. \tag{2.10}$$

It is important to note that (2.10) should be consistent with the limiting behaviours in the case of no ambient turbulence and the case in which the turbine-induced turbulence effect is negligible. In the case of no ambient turbulence, (2.10) should yield the mixing layer growth relation, i.e. (2.5). With the same argument and by neglecting the turbine-induced turbulence contribution, (2.10) should provide the same form as (1.3). In order to satisfy these limiting behaviours, we can rewrite the right-hand side of (2.10) as follows:

$$\sigma_{ey}(t)\frac{\mathrm{d}\sigma_{ey}(t)}{\mathrm{d}t} = \underbrace{\sqrt{Sc_t}\langle v_{(T/\beta)}^2\rangle^{1/2}\sigma_{ey}(t)}_{\text{Ambient flow}} + \underbrace{S'\Delta U_{max}\sigma_{ey}(t)}_{\text{Turbine-induced}}, \tag{2.11}$$

where ΔU_{max} is the shear velocity at each downstream location and equal to $U_\infty - U_{centre}(x)$, in which $U_{centre}(x)$ is the wake centreline velocity. The turbulent Schmidt number of 0.5 is proposed for mixing layers (Reynolds 1976). $\langle v_{(T/\beta)}^2\rangle^{1/2}$ is the root-mean-square of the lateral direction velocity component sampled upstream of the turbine at hub level and filtered in time using a moving average filter with the window size equal to T/β, with T being the travel time. At short travel time, all the eddies contribute to the wake growth. By moving downstream and increasing the travel time, the contribution of small eddies decreases, and only eddies with size equal and larger than the wake contribute to the wake expansion. Therefore, by filtering at each downstream distance, the model ensures that only the contribution of effective turbulence scales is considered. Following the derivation presented by Zong & Porté-Agel (2020) for the wake advection

velocity, $U_{adv}(x) = 0.5(U_{centre}(x) + U_\infty)$, one can transform (2.11) to the spatial notation:

$$\frac{\mathrm{d}\sigma_{ey}}{\mathrm{d}x} = \sqrt{Sc_t}\frac{\langle v^2_{(T/\beta)}\rangle^{1/2}}{U_{adv}(x)} + S'\frac{\Delta U_{max}(x)}{U_{adv}(x)}, \tag{2.12}$$

which can also be written in the integral form

$$\int_{\sigma_{ey(x_0)}}^{\sigma_{ey(x)}} \mathrm{d}\sigma_{ey} = \sqrt{Sc_t}\langle v^2_{(T/\beta)}\rangle^{1/2}\int_{x_0}^{x}\left(\frac{\mathrm{d}x}{U_{adv}(x)}\right) + S'\int_{x_0}^{x}\left(\frac{\Delta U_{max}(x)}{U_{adv}(x)}\right)\mathrm{d}x. \tag{2.13}$$

As the mixing layer starts to grow from the end of the expansion region (x_0), the lower bound of the integral is equal to zero. The travel time (T) can be calculated as

$$T = \int_{x_0}^{x}\left(\frac{\mathrm{d}x}{U_{adv}(x)}\right). \tag{2.14}$$

In order to have a compact form of (2.13), one can solve for $U_{centre}(x)$ from the definition of the advection velocity to rewrite the shear velocity term as $\Delta U_{max}(x) = 2(U_\infty - U_{adv}(x))$. By integrating the turbine-induced term on the right-hand side, we can derive a simplified form of (2.13) as follows:

$$\sigma_{ey}(x) = \sqrt{Sc_t}\langle v^2_{(T/\beta)}\rangle^{1/2}T + 2S'(U_\infty T - (x - x_0)). \tag{2.15}$$

It should be noted that this form of the spreading equation for σ_{ey} considers both the effects of the effective incoming turbulent eddies (by filtering the velocity time series at each downwind location) and the turbine-induced turbulence on the wake width. The starting location for the spreading equation, x_0, is where the centreline velocity has decreased from the rotor plane value to its minimum and theoretical value of $U_\infty\sqrt{1 - C_T}$. The value of x_0 is usually assumed to be one rotor diameter based on experimental observation (Krogstad & Adaramola 2012) and one-dimensional momentum theory (Hansen 2015) for a turbine operating in the optimal tip speed ratio. This assumption is consistent with the concept of expansion region proposed by Crespo *et al.* (1999). In the expansion region, the pressure builds up to reach the ambient pressure, and the shear layer growth is negligible compared with the rotor diameter. Figure 3 presents a schematic of the mixing layer growth, and the wake velocity profile transformation from a top-hat shape in the near wake to a self-similar Gaussian profile in the far wake. At each downstream location, an estimation of the wake centreline velocity is required. In the self-similar region of the wake, this value is calculated from the Gaussian wake model derived based on mass and momentum conservation (Bastankhah & Porté-Agel 2014):

$$\frac{U_{centre}(x)}{U_\infty} = \sqrt{1 - \frac{C_T}{8(\sigma_{wake}(x)/d)^2}}. \tag{2.16}$$

In the near-wake region, with the help of one-dimensional momentum theory (Hansen 2015), it can be shown that the normalised wake centreline velocity should not fall below $\sqrt{1 - C_T}$. As in this region the wake does not reach the full self-similar Gaussian shape, (2.16) is not valid and either diverges or yields values less than $\sqrt{1 - C_T}$. Therefore, the normalised wake centreline velocity is set to $\sqrt{1 - C_T}$ in the near-wake region (Abkar, Sørensen & Porté-Agel 2018).

As at each downstream location the centreline velocity is not known prior to the mixing layer characteristic length, one should deploy an iterative method between (2.15)

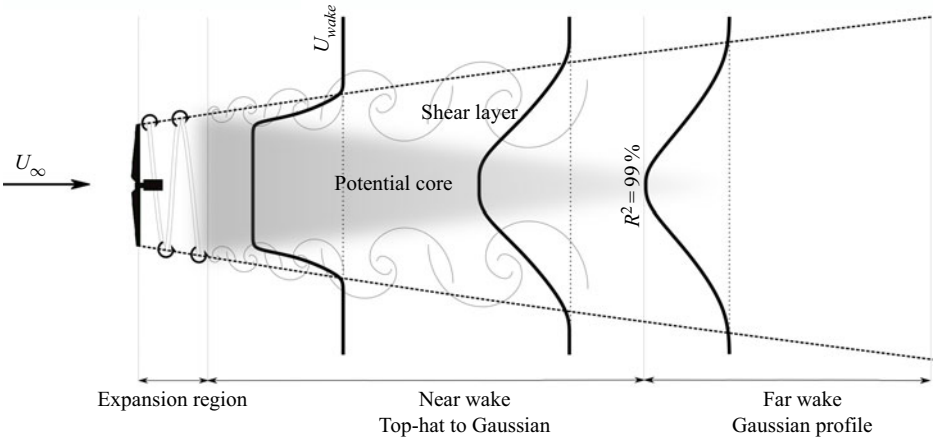

Figure 3. Schematic of the gradual growth of the mixing layer from the wake edge and the wake velocity distribution from the near wake (top-hat) to the far wake (self-similar Gaussian).

(including the travel time calculation (2.14) and filtering) and (2.16). Technically, at each downstream location, the U_{centre} is initialised with the previous location value to have an initial estimation of the advection velocity, travel time and filtered velocity to solve (2.15). The estimated length scale is then used to update the centreline velocity. This iterative procedure is repeated until convergence. As the velocity deficit in the wake has a smooth decreasing form, the computational cost of the iterative process is insignificant. A key step of the new framework is the estimation of σ_{wake} (Gaussian wake width) based on the mixing layer characteristic length (σ_e). For this purpose, we profit from the presented analogy between wind turbine wake expansion and scalar diffusion from a continuous disk source in § 2.1.3 to correlate the mixing layer characteristic length (σ_e) and the Gaussian profile standard deviation (σ_{wake}) at each downstream location. Therefore, by using this relation (equation (2.8)) the model is closed.

All the aforementioned derivations were based on the lateral velocity component. However, there is no limitation to extend the methodology to the vertical direction by replacing $\langle v^2_{(T/\beta)}\rangle^{1/2}$ with $\langle w^2_{(T/\beta)}\rangle^{1/2}$. Several numerical and experimental studies have shown that despite the differences between $\langle v^2\rangle$ and $\langle w^2\rangle$ in the ABL, wind turbines wakes are fairly axisymmetric and they can be represented by an equivalent wake width that can be defined as the geometrical mean of wake widths in the spanwise and vertical directions ($\sigma_{wake,tot} = \sqrt{\sigma_{wake,y}\sigma_{wake,z}}$) (Abkar & Porté-Agel 2015; Xie & Archer 2015; Cheng & Porté-Agel 2018).

In summary, in order to calculate the wake width at each downwind location, one should solve (2.15), along with the travel time (2.14) and centreline velocity (2.16) while using (2.8) to correlate the mixing layer characteristic length to the wake width. The primary input for the new wake model is a velocity time series sampled upstream of the turbine at hub height. Within the framework of the current study, this signal is sampled from LESs of a fully developed turbulent flow under neutral atmospheric conditions.

2.3. *Near-wake length*

In this section, we derive a new relation for the near-wake length based on the incoming atmospheric turbulence and turbine operating conditions. For the model presented in

§ 2.2, one should calculate the near-wake length before solving (2.15). As mentioned earlier, in the near-wake region, one can assume that the centreline velocity is constant ($U_{centre} = U_\infty\sqrt{1 - C_T}$). By this assumption, the advection and shear velocity can be simplified as a function of the free-stream velocity and turbine operating condition:

$$\left.\begin{array}{c} U_{adv} = 0.5(U_\infty + U_{centre}) = 0.5U_\infty(1 + \sqrt{1 - C_T}), \\ \Delta U_{max} = U_\infty - U_{centre} = U_\infty(1 - \sqrt{1 - C_T}). \end{array}\right\} \tag{2.17}$$

Moreover, to include the lateral and vertical velocity components contribution to the near-wake length, based on the axisymmetric growth of the turbine wakes, one possible approach is to introduce the equivalent filtered velocity as the geometrical mean of the lateral and vertical components. By applying these assumptions to (2.13), the spreading equation can be written as follows:

$$\sigma_{e,NW} = \frac{1}{U_{adv}}(\sqrt{Sc_t}\sqrt{\langle v^2_{(T/\beta)}\rangle^{1/2}\langle w^2_{(T/\beta)}\rangle^{1/2}} + S'\Delta U_{max})(x_{NW} - x_0), \tag{2.18}$$

where x_{NW} is the length of the near wake, $\sigma_{e,NW}$ is the mixing layer characteristic length at the end of the near wake, and x_0 represents the expansion region length ($\approx 1d$). By solving (2.18) for x_{NW}, the following relation is obtained for the near-wake length:

$$\frac{x_{NW}}{d} = \frac{\sigma_{e,NW}}{d}\frac{U_\infty(1 + \sqrt{1 - C_T})}{2(\sqrt{Sc_t}\sqrt{\langle v^2_{(T/\beta)}\rangle^{1/2}\langle w^2_{(T/\beta)}\rangle^{1/2}} + U_\infty S'(1 - \sqrt{1 - C_T}))} + \frac{x_0}{d}. \tag{2.19}$$

This equation provides an estimation of the near-wake length based on the incoming ambient turbulence and turbine operating conditions. By including the filtered velocity components, one ensures that the relevant scales of the incoming turbulence are contributing to the wake growth rate until the end of the near wake. Since the corresponding travel time is not known prior to the near-wake length, an iterative method should be used to solve (2.19). In order to avoid the iterative method of (2.19) for the near-wake length calculation, one can introduce the following simplifications for (2.19) to provide simpler forms to estimate the near-wake length based on the following assumptions.

- As the near-wake region is relatively close to the turbine and the travel time is small, one can assume that all the turbulence scales contribute to the wake expansion in that region. By this assumption, one can approximate $\langle v^2_{(T/\beta)}\rangle^{1/2}$ ($\langle w^2_{(T/\beta)}\rangle^{1/2}$) as $I_v U_\infty$ ($I_w U_\infty$) where I_v (I_w) is the lateral (vertical) turbulence intensity. Therefore, (2.19) can be rewritten as

$$\frac{x_{NW}}{d} = \frac{\sigma_{e,NW}}{d}\frac{1 + \sqrt{1 - C_T}}{2(\sqrt{Sc_t}(\sqrt{I_v I_w}) + S'(1 - \sqrt{1 - C_T}))} + \frac{x_0}{d}. \tag{2.20}$$

- For the particular case of near-neutral atmospheric conditions, the standard deviation of the three velocity components can be scaled with the friction velocity ($\sigma_u \approx 2.5u_*$, $\sigma_v \approx 1.9u_*$, $\sigma_w \approx 1.3u_*$) in the surface layer (Panofsky 1984). These scalings are only valid in the neutral surface layer. Therefore, under neutral conditions, we can further simplify (2.20) as follows:

$$\frac{x_{NW}}{d} = \frac{\sigma_{e,NW}}{d}\frac{1 + \sqrt{1 - C_T}}{2(\sqrt{Sc_t}(0.63I_u) + S'(1 - \sqrt{1 - C_T}))} + \frac{x_0}{d}. \tag{2.21}$$

In order to estimate the near-wake length with (2.19)–(2.21), the value of $\sigma_{e,NW}/d$ should be specified. As shown in figure 2(*a*) and discussed in § 2.1.3, the R^2 reaches to 0.99 for $\sigma_e/d \approx 0.18$. The $R^2 = 0.99$ criterion is often used as a threshold to determine the onset of the self-similar Gaussian behaviour of the far wake in experimental (Carbajo Fuertes *et al.* 2018) and numerical studies (Sørensen *et al.* 2015). Therefore, by using $\sigma_{e,NW}/d \approx 0.18$, (2.19)–(2.21) are closed relations.

2.4. *Simplified form of spreading equation*

In this section, we aim to find a simplified form of the filtering operator in (2.15) and present a computationally faster implementation for the wake width calculation with a reasonable accuracy. As stated by (2.1), the original form of Taylor diffusion theory is based on the velocity ACF. As a well-known approximation (Taylor 1922; Neumann 1978; Hanna *et al.* 1982), ACF can be written in a simple exponential form:

$$R(T) = \exp\left(-\frac{T}{T_L}\right), \tag{2.22}$$

in which T is the travel time from the source and T_L is the Lagrangian integral time scale. By replacing (2.22) in (2.1), performing the integration for the lateral velocity component, and introducing the Lagrangian integral time scale for the lateral velocity time series as T_{Lv}, the following form for the particle distribution behind a source is derived:

$$\sigma_y^2(T) = 2\sigma_v^2 T T_{Lv} - 2\sigma_v^2 T_{Lv}^2\left(1 - \exp\left(\frac{-T}{T_{Lv}}\right)\right). \tag{2.23}$$

From a practical point of view, fixed-point measurements are more feasible than particle tracking methods to estimate the diffusion properties. Therefore, to calculate the Lagrangian integral time scale, one can estimate the integral time scale from a fixed point time series measurement (based on the definition used by Hanna (1981), the integral time scale is equal to the time lag where the ACF first drops to $1/e$) and then use the previously defined scale factor β. Following the derivation presented in Pasquill & Smith (1983), one can write the particle distribution as a function of the travel time and filtered velocity:

$$\sigma_y^2(T) = \langle v_{(T/\beta)}^2\rangle T^2. \tag{2.24}$$

By equating (2.23) and (2.24), the lateral filtered velocity for each travel time can be written as follows:

$$\langle v_{(T/\beta)}^2\rangle^{1/2} = \frac{\sigma_v T_{Lv}}{T}\sqrt{2\left(\frac{T}{T_{Lv}} - \left(1 - \exp\left(\frac{-T}{T_{Lv}}\right)\right)\right)}, \tag{2.25}$$

where σ_v is the standard deviation of the lateral velocity component. Therefore, the simplified version of spreading (2.15) for the lateral mixing layer characteristic length (σ_{ey}) can be written as follows:

$$\sigma_{ey}(x) = \underbrace{T\sqrt{Sc_t}\frac{\sigma_v T_{Lv}}{T}\sqrt{2\left(\frac{T}{T_{Lv}} - (1 - \exp(\frac{-T}{T_{Lv}}))\right)}}_{\text{Ambient flow}} + \underbrace{2S'(U_\infty T - (x - x_0))}_{\text{Turbine-induced}}. \tag{2.26}$$

One can simplify the travel time in the ambient flow term to have a more compact form:

$$\sigma_{ey}(x) = \underbrace{\sqrt{Sc_t}\sigma_v T_{Lv}\sqrt{2\left(\frac{T}{T_{Lv}} - \left(1 - \exp\left(\frac{-T}{T_{Lv}}\right)\right)\right)}}_{\text{Ambient flow}} + \underbrace{2S'(U_\infty T - (x - x_0))}_{\text{Turbine-induced}}. \quad (2.27)$$

Equation (2.27) can be used instead of (2.15) to calculate the lateral mixing layer characteristic length with a simpler method that does not require explicit filtering of the velocity time series by an external function. The range of validity of (2.27) is the same as that of the model presented in § 2.2; one can solve (2.27) from the end of the expansion region (x_0) until the desired downwind distance. At each downstream location, the travel time is calculated from (2.14), the centreline velocity is either constant (near wake) or calculated from the Gaussian wake model (far wake), and the mixing layer characteristic length and the Gaussian wake width are correlated through (2.8). As in the model presented in § 2.2, there is no limitation to extend (2.27) to the vertical direction with the respective properties. This equation can be solved easily without any external function for filtering the velocity time series, and predicts the wake width in a fast and easy to implement manner.

2.5. *Near-wake treatment: a new form for the velocity deficit distribution*

This section focuses on introducing a new formulation for the super-Gaussian shape function to predict the wake velocity deficit distribution in the near wake. By definition, the super-Gaussian shape function allows the transition from a top-hat distribution to a Gaussian profile with a single functional form. Based on the presented analogy of wind turbine wake expansion and scalar diffusion from a disk source, the goal is to propose a new method to determine the super-Gaussian shape function parameters for the near-wake velocity deficit distribution that asymptotes to the Gaussian wake model in the far wake. It should be noted that the derivation presented in the following closely follows the steps proposed by Blondel & Cathelain (2020). We start by assuming that the non-dimensional wake velocity deficit has a super-Gaussian form:

$$\frac{\Delta U(x)}{U_\infty} = C'(x) f(x, r) = C'(x) \exp\left(-\frac{r^{n(x)}}{2\sigma'^2(x)}\right), \quad (2.28)$$

where $C'(x)$ is the wake maximum velocity deficit, $f(x, r)$ is the shape function, r is the radial distance from the wake centre, $n(x)$ is the smoothness parameter and $\sigma'(x)$ is the super-Gaussian wake width (when $n = 2$, $\sigma'(x)$ is the wake standard deviation). By neglecting the viscous and pressure terms in the momentum equation, the following integral can be derived for conserving mass and momentum (Tennekes & Lumley 1972):

$$2\pi\rho \int_0^\infty U_w(U_\infty - U_w) r \, \mathrm{d}r = T, \quad (2.29)$$

where ρ is the air density and T is the turbine thrust force. By replacing (2.28) in (2.29) and integrating, the following relation between the maximum velocity deficit, super-Gaussian wake width, smoothness parameter and turbine thrust coefficient is derived including the

Gamma function (Γ):

$$C'^2(x) - 2^{2/n(x)}C'(x) + \frac{n(x)C_T}{16\Gamma(2/n(x))\sigma'^{4/n(x)}} = 0. \tag{2.30}$$

Within the framework of the presented analytical model (§ 2.2), the maximum velocity deficit is known after solving the model at each downstream location. However, the smoothness parameter and the super-Gaussian wake width are not known. In order to define a super-Gaussian shape function that predicts the velocity deficit distribution in the near wake and converges to a self-similar Gaussian profile in the far wake, we propose a new expression for the smoothness parameter. The choice of the smoothness parameter is made to guarantee that the super-Gaussian prediction smoothly transitions to a self-similar Gaussian distribution in the far wake ($n(x) = 2$), which is consistent with the aforementioned Gaussian model results in that region. In addition, one should consider that the near-to-far-wake transition occurs at different downwind locations based on the incoming flow turbulence level. In order to fulfil the conditions listed above, we propose the following form for the smoothness parameter variation in the wind turbine wake:

$$n(x) = 2 + A\,\mathrm{erfc}\left(\frac{2(\sigma_e(x)/d)}{0.18}\right), \tag{2.31}$$

where $\sigma_e(x)/d$ is the total mixing layer characteristic length (geometrical mean of the lateral and vertical characteristic lengths) at each downwind location, 0.18 corresponds to the near-wake criterion introduced in § 2.3 and A is a tunable parameter which defines the smoothness of the super-Gaussian profile at the end of expansion region ($n(x_0) = 2 + A$). This form ensures that the smoothness parameter converges to two in the far wake and the super-Gaussian shape function switches to the Gaussian wake model. At this point, with the smoothness and maximum velocity deficit known at each downstream location, one can solve (2.30) for the super-Gaussian wake width:

$$\sigma'(x) = \left(\frac{n(x)C_T}{2^{2/n(x)}C'(x) - C'^2(x)}\frac{1}{16\Gamma(2/n(x))}\right)^{(n(x)/4)}. \tag{2.32}$$

Therefore, by calculating the super-Gaussian wake width at each downstream location, the super-Gaussian shape function is fully defined and can provide the wake velocity deficit distribution in the near wake and provides the correct asymptotic behaviour in the far wake.

3. Model validation

3.1. *LES framework*

To validate the model and test its performance, a series of LESs of a utility-scale wind turbine wake under neutral ABL conditions were performed with the in-house LES code developed at the WiRE Laboratory of EPFL (WiRE-LES). The code solves the filtered incompressible Navier–Stokes equation:

$$\frac{\partial \tilde{u}_i}{\partial x_i} = 0, \tag{3.1}$$

$$\frac{\partial \tilde{u}_i}{\partial t} + \tilde{u}_j\frac{\partial \tilde{u}_i}{\partial x_j} = -\frac{\partial \tilde{p}^*}{\partial x_i} - \frac{\partial \tau_{ij}}{\partial x_j} - f_i, \tag{3.2}$$

where $i = 1, 2, 3$ refers to the streamwise, spanwise and vertical directions, respectively, $\tilde{u}$ is the filtered velocity, $\tilde{p}^*$ is the filtered modified kinematic pressure, τ is the kinematic

Case	$z_0(m)$	I_u	I_v	I_w
1	5×10^{-1}	0.140	0.097	0.074
2	5×10^{-2}	0.099	0.071	0.055
3	5×10^{-3}	0.077	0.055	0.043
4	5×10^{-4}	0.062	0.044	0.034
5	5×10^{-5}	0.053	0.038	0.029

Table 1. Incoming turbulence intensity of LES cases at turbine hub height: I_u, I_v and I_w denote the streamwise, spanwise and vertical turbulence intensities, respectively, and z_0 corresponds to the surface roughness.

sub-grid scale (SGS) stress and f represents the additional effects such as an external forcing to drive the flow or the turbine forces. The code is based on pseudo-spectral schemes in the horizontal directions and second-order centred finite-difference scheme in the vertical direction. The horizontal boundary conditions are periodic, a flux-free boundary condition is used at the top, and the bottom boundary condition is set through the local application of the Monin–Obukhov similarity theory. For time advancement, the second-order Adams–Bashforth explicit scheme is used. Within the WiRE-LES framework, the Lagrangian scale-dependent dynamic model (Stoll & Porté-Agel 2006) is used to parametrise the SGS turbulent fluxes and the rotational actuator disk model is used to model the turbine-induced forces (Wu & Porté-Agel 2011). The WiRE-LES has been validated in several studies of ABL flows with the presence of wind turbines (Porté-Agel *et al.* 2011; Wu & Porté-Agel 2011; Porté-Agel, Wu & Chen 2013; Revaz & Porté-Agel 2021).

In this study, a domain size of $L_x = 3840$ m, $L_y = 1920$ m, $L_z = 955$ m is uniformly divided into $N_x = 256$, $N_y = 192$, $N_z = 192$ grid points. The simulations, as listed in table 1, cover a wide range of incoming turbulence levels and are driven by a constant streamwise pressure gradient up to $0.8L_z$ to maintain a hub height velocity of 8 m s^{-1}. To minimise the effect of the top boundary on the flow, no forcing is applied in the top 20 % of the domain. The inflow is generated through a set of precursor simulations and imposed on the simulations with the turbine. The wind turbine has a diameter of 80 m and a hub height of 70 m and is placed 12 rotor diameters after the inlet. In this condition, the turbine has an almost constant thrust coefficient of 0.8. To avoid numerical instabilities, the parametrised turbine forces are distributed smoothly on the computational grid with the help of a Gaussian kernel (Mikkelsen 2003). To guarantee mesh independent results, the grid spacing is chosen to cover the rotor diameter with 8 points in the spanwise direction and 16 points in the vertical direction. These values satisfy the minimum grid points required in the spanwise direction (at least five cells) and vertical direction (at least seven cells) across the rotor diameter (Wu & Porté-Agel 2011, 2012).

3.2. *Results and discussion*

In this section, we assess the performance of two forms of the new analytical model (hereafter, 'Model Filter' is used to denote the form presented in § 2.2, whereas the simplified form presented in § 2.4 is denoted as 'Model ITS' in which ITS stands for integral time scale) by comparing its predictions against results from LESs of the wake of a utility scale wind turbine. Several cases are considered, corresponding to a wide range of turbulence intensities in the incoming flow under neutral atmospheric conditions,

as summarised in table 1. For all the LES cases, the simulated wake velocity deficit distribution is fitted with a Gaussian profile in the lateral direction and a Gaussian profile with ground reflection in the vertical direction. As discussed earlier, wind turbine wakes are fairly axisymmetric with similar growth rates in the lateral and vertical directions (Cheng & Porté-Agel 2018). Therefore, the geometrical mean of the lateral and vertical wake widths is considered as the total wake width ($\sigma_{wake,tot} = \sqrt{\sigma_{wake,y}\sigma_{wake,z}}$). In order to compare the LES results with the predictions from the new analytical model, the latter uses as input the incoming flow information from a velocity time series sampled during the LES simulations, upstream of the turbine at hub level. Using the incoming flow information, the model computes the total wake width at each downwind distance. It should be mentioned that Model Filter and Model ITS can estimate the total wake width from $1d$ to the desired downwind distance. For this study and the mentioned cases, both models are used in the range of $1d$ to $20d$. Regarding the model parameters, $Sc_t = 0.5$ (Reynolds 1976), $S' = 0.043$ (§ 2.1.2), $x_0/d = 1$ (§ 2.2) and $\sigma_{e,NW}/d = 0.18$ (§ 2.1.3), are used based on the presented discussions in § 2, without any parameter tuning.

Figure 4 shows a comparison of the wake width as a function of the downwind distance computed from the new analytical model, the empirical wake growth rate relations proposed by Niayifar & Porté-Agel (2016) and Teng & Markfort (2020), and that obtained from the LES data. As shown in this figure, the proposed model can predict the wake width reasonably well within a wide range of incoming turbulence levels. In comparison with the empirical relations of the wake growth rate (with different tuned parameters), the model shows a reasonable prediction across a wide range of turbulence levels. As can be noted from figure 4, the wake growth rate relation proposed by Niayifar & Porté-Agel (2016) provides reasonable wake width predictions in comparison with the LES data, whereas the relation proposed by Teng & Markfort (2020) underestimates the wake width in the presence of low turbulence intensity in the incoming flow. The new physics-based model captures the start of the wake expansion at the beginning of the far wake, followed by an approximately linear growth rate with the downwind distance. At farther downstream distances (greater than around $12d$, depending on the atmospheric turbulence level), the wake expansion rate gradually decreases from the initial linear growth rate. This is due to the fact that, by increasing downstream distance, the range of effective ambient turbulence scales contributing to the wake expansion (i.e. turbulent eddies of size equal or larger than the wake width) decreases. The proposed model can capture that effect and the associated nonlinear wake expansion rate, which is crucial for the prediction of wind farm wakes using analytical wake models. Moreover, figure 4 highlights the importance of including the effect of turbine-induced turbulence on the turbulent viscosity. By including this term, the model provides an acceptable prediction and avoids the underestimation of the wake growth rate associated with the use of only atmospheric turbulence in the definition of the turbulence viscosity (Cheng & Porté-Agel 2018).

Figure 5 shows the change of the maximum normalised velocity deficit, at the turbine hub height, as a function of downwind distance computed from the new analytical model, the Gaussian wake model with the empirical wake growth rate relations proposed by Niayifar & Porté-Agel (2016) and Teng & Markfort (2020), and that obtained from LES data. As shown in this figure, the model can predict the maximum wake velocity deficit in a wide range of incoming turbulence levels reasonably well. Note that the assumption of the expansion region downstream of the turbine and the uniform velocity distribution in the near-wake region is consistent with the LES results. The maximum velocity deficit has an approximately uniform distribution in the near wake and decreases gradually after the near-to-far-wake transition point (shown in figure 5 as 'Near-wake LES'). The comparison between the LES data and the wake velocity deficit predicted by the Gaussian model using

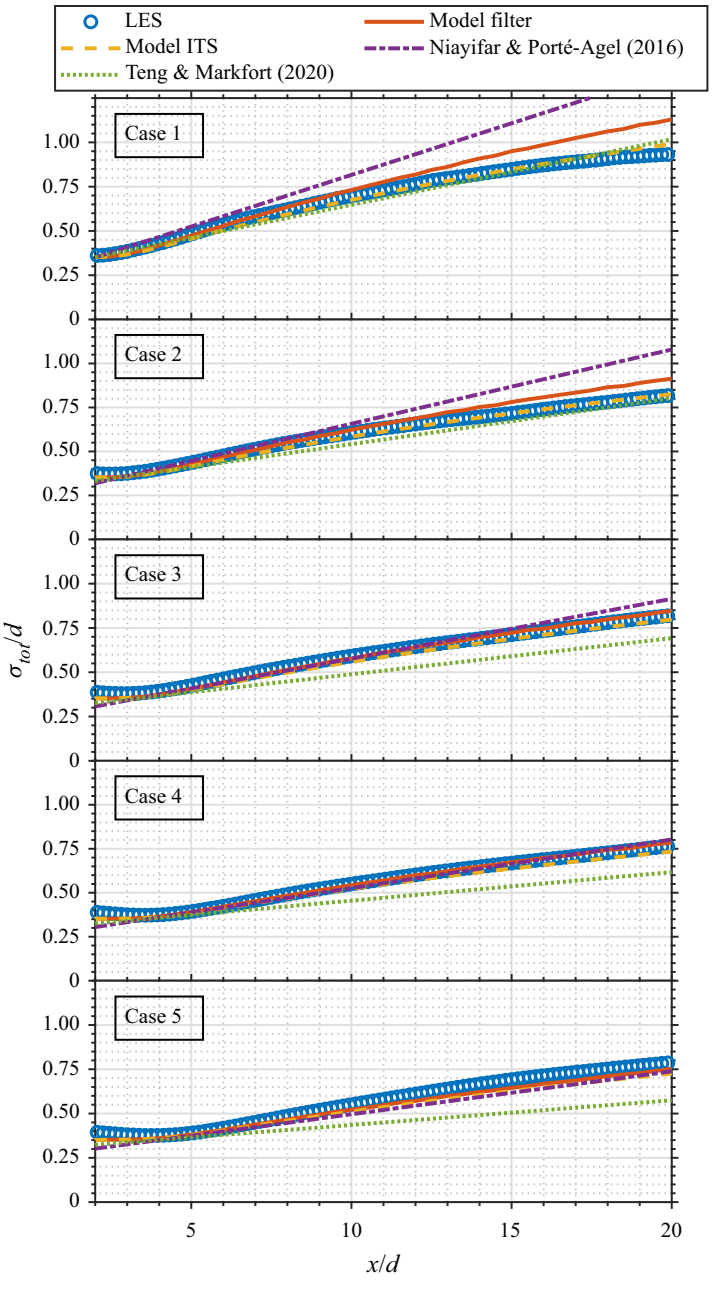

Figure 4. Normalised total wake width as a function of streamwise distance. The circles indicate LES results, the solid lines are the solution obtained from Model Filter as presented in § 2.2 and the dashed lines are the solution from the simplified approach, Model ITS in § 2.4. The prediction by the empirical wake growth rate relations proposed by Niayifar & Porté-Agel (2016) and Teng & Markfort (2020) are also shown.

the empirical relations for the wake growth rate shows the sensitivity of the predictions to the empirical constant. The Gaussian wake model with the proposed relation by Niayifar & Porté-Agel (2016) can provide reasonable predictions for the wake velocity deficit, whereas using the relation by Teng & Markfort (2020) overestimates the wake velocity deficit in

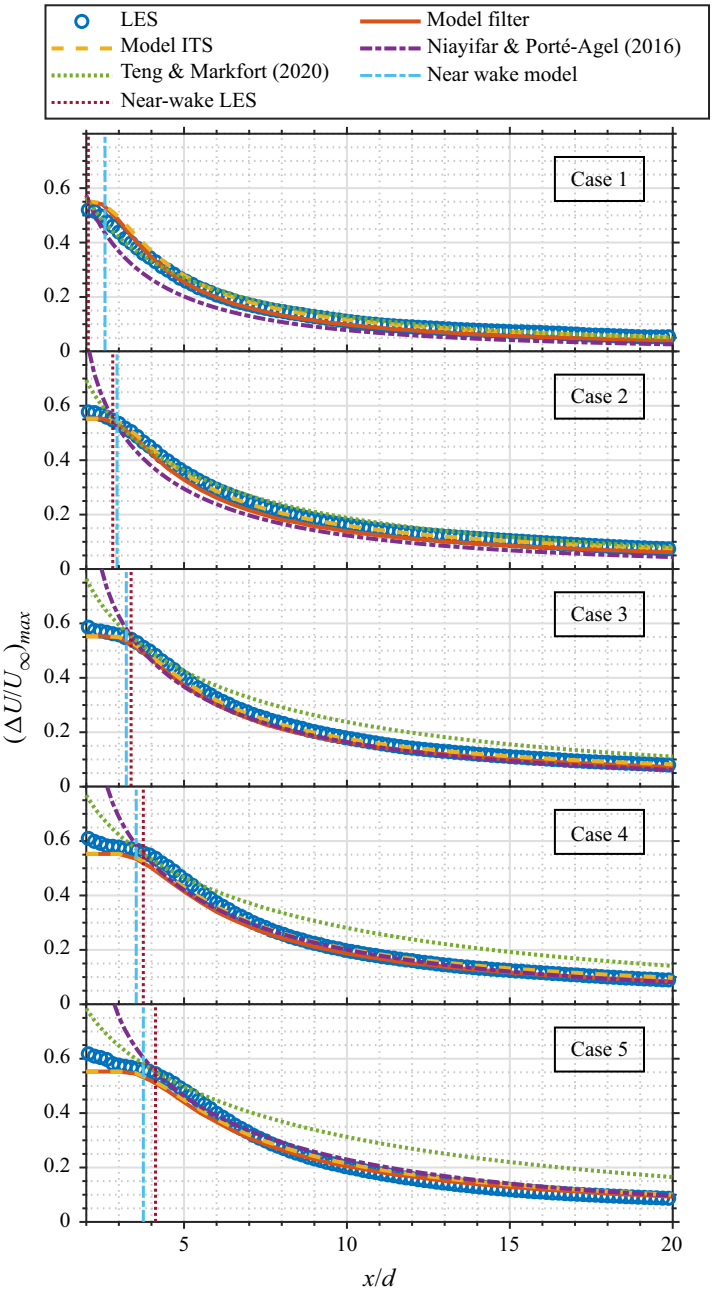

Figure 5. Normalised maximum velocity deficit as a function of streamwise distance. The vertical dotted line corresponds to the near-wake length from LES cases and the vertical dash-dotted line corresponds to the near-wake length obtained from (2.19). For the legend refer to the caption of figure 4.

the presence of low turbulence intensity in the incoming flow. In addition, figure 5 shows a comparison between the near-wake length of the LES cases and the near-wake length of the model, which is discussed in more detail later in this section. As can be noted in figures 4 and 5, Model Filter and Model ITS can predict the wake growth rate and the

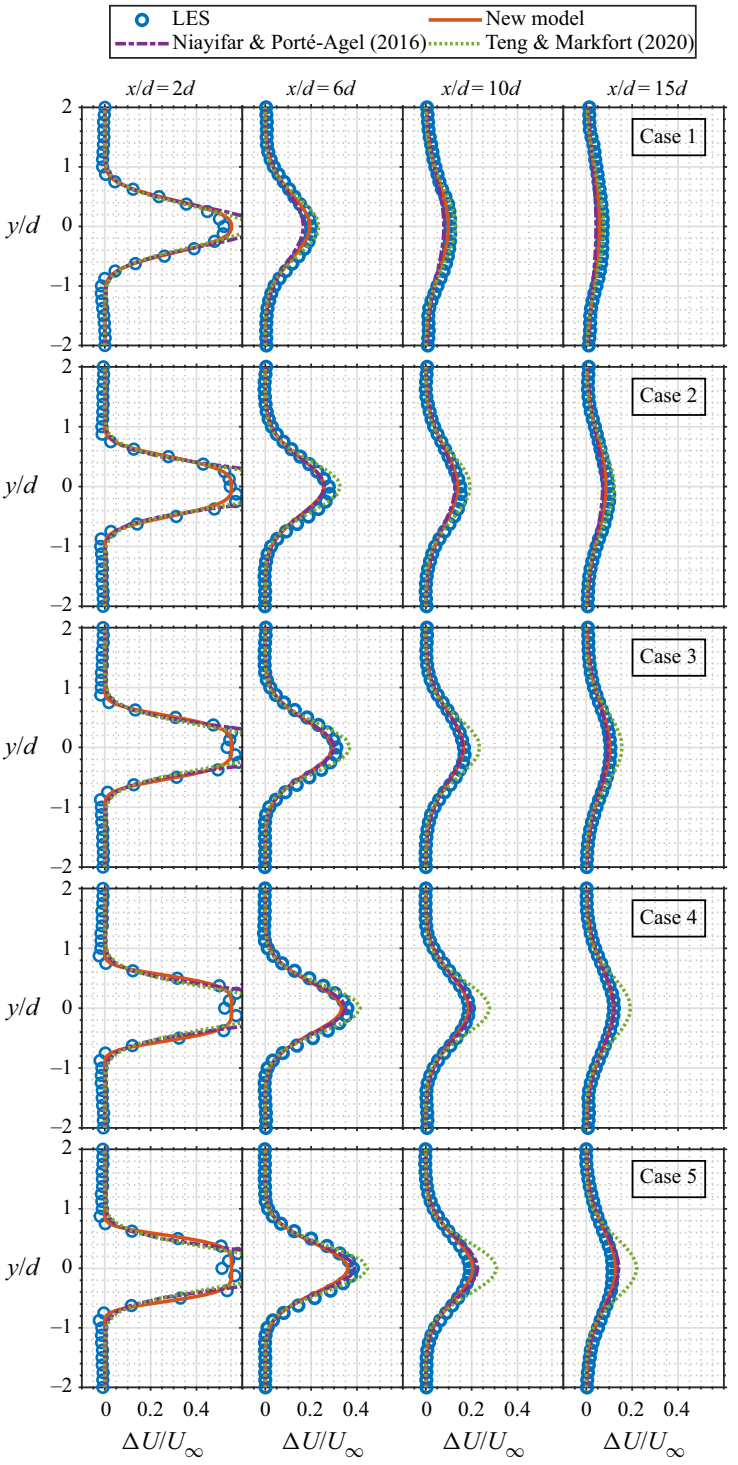

Figure 6. Normalised velocity deficit profiles at different streamwise locations for all the cases.

maximum wake velocity deficit downstream of the turbine reasonably well. There exist slight differences between the two methods due to the different approaches to compute the standard deviation of the filtered velocity. Based on the presented results, one can conclude that the proposed model can provide fast and reasonably accurate predictions of the wake width under a wide range of incoming turbulence conditions.

Figure 6 shows a comparison of the lateral profiles of the normalised velocity deficit downwind of the turbine at hub level calculated by the proposed model, the Gaussian wake model with the empirical wake growth rate relations proposed by Niayifar & Porté-Agel (2016) and Teng & Markfort (2020), and those obtained from the simulations. It should be noted that the new analytical model, as presented in § 2.2, uses the Gaussian wake model to calculate the wake velocity deficit profiles in the far wake (figure 6, $x/d = 6, 10, 15$). In the near wake (figure 6, $x/d = 2$), the wake velocity deficit profiles are calculated using the new super-Gaussian form as presented in § 2.5. The proposed framework allows the calculation of the wake velocity deficit profiles in the near wake with the super-Gaussian form consistent with the Gaussian wake model by ensuring the super-Gaussian smoothness parameter (n) is equal to two in the far-wake region. For the reported results, the value of the super-Gaussian model parameter (A) is set to 12. It is worth mentioning that the optimum value of A could depend on the turbine operating condition (C_T) and it is not universal. As shown in the figure, in the near wake, the new super-Gaussian form predicts the wake velocity deficit distribution reasonably well (figure 6, $x/d = 2$). These detailed comparisons within a wide range of incoming turbulence conditions, as shown in figures 4, 5 and 6, validate the new analytical model.

As discussed in § 2.2, the wake advection velocity at each downwind location is not known prior to the wake width and wake centreline velocity, and one should deploy an iterative scheme to calculate these quantities at each downstream location. In addition to the definition of wake advection velocity presented in this study, other approaches have been used to estimate this quantity. For example, in the dynamic wake meandering model (Larsen *et al.* 2008), the wake advection velocity is assumed to be equal to the free stream velocity ($U_{adv} = U_\infty$). In order to explore how different values of the wake advection velocity affect the new analytical model outputs, we compare the model results, as presented in § 2.2, for four different approaches to calculate the advection velocity: (1) $U_{adv}(x) = 0.5(U_\infty + U_{centre}(x))$, (2) $U_{adv}(x) = U_\infty$, (3) $U_{adv}(x) = 0.5U_\infty(1 + \sqrt{1 - C_T}) \xrightarrow{C_T=0.8} U_{adv}(x) = 0.72U_\infty$ and (4) $U_{adv}(x) = 0.5(0.72U_\infty + U_\infty) = 0.86U_\infty$. These approaches cover the original formulation of the advection velocity in the new model (approach 1), the constant advection velocity proposed by the dynamic wake meandering model (approach 2) and the constant advection velocity equal to the average of the free stream and theoretical near-wake centreline velocity from one-dimensional momentum theory (approach 3). For the last approach, the advection velocity is defined as the average of approaches 2 and 3, allowing us to analyse the model outputs in the middle of these two limits. Figure 7 shows the change of the maximum normalised velocity deficit, at the turbine hub level, as a function of normalised downwind distance for the proposed approaches and that obtained from LES data. As can be noted, all the approaches provide similar asymptotic behaviour in the very far wake at downstream distances greater than $12d$. For shorter distance from the turbine, the assumption of $U_{adv} = U_\infty$ provides an overly fast advection of the wake that results in a shorter travel time for a fixed downwind distance compared with the LES results. As a result, and as shown in figure 7, this assumption causes an overly slow wake recovery and a clear overestimation of the wake velocity deficit in the far wake up to downstream distances of about six to eight rotor diameters (depending on the atmospheric turbulence level) in

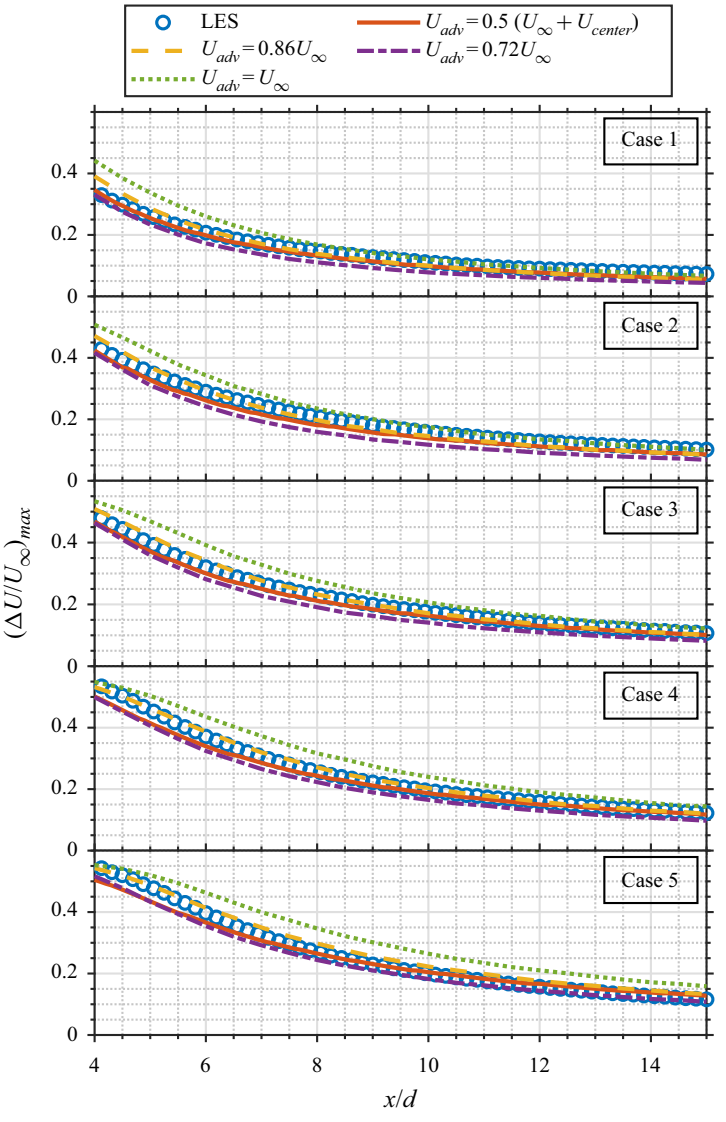

Figure 7. Normalised maximum velocity deficit as a function of streamwise distance in the far wake, comparison of four different approaches to calculate the advection velocity.

comparison with the LES results. On the other hand, the assumptions of $U_{adv} = 0.72U_\infty$ and $U_{adv} = 0.86U_\infty$ provide predictions of the maximum wake velocity deficit that are closer to those obtained with LES simulations. This can be explained by the fact that, for those distances, these values are closer to the expected advection velocity reported in the literature and defined in § 2.2. Therefore, the approach for estimating the advection velocity can influence the wake velocity deficit prediction, particularly in the far wake up to downwind distances of about six to eight rotor diameters.

Next, we use the model to analyse the contribution of each term to the wake width in more detail. Figure 8 shows the average contribution of the ambient and the turbine-induced turbulence to the total wake width calculated with the new model as a function of radial turbulence intensity ($\sqrt{I_v I_w}$). The relative contribution of each term

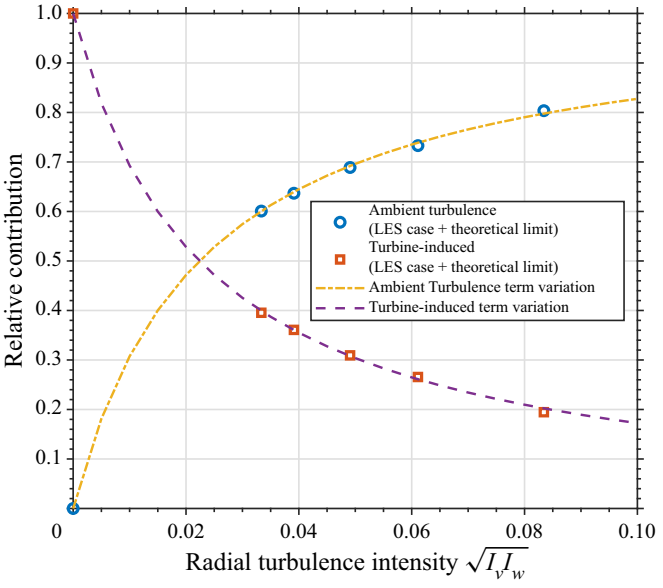

Figure 8. Relative contribution of the ambient (circle) and turbine-induced (square) turbulence to the total wake width computed with the new model as a function of radial turbulence intensity. The theoretical limits in the extreme of no ambient turbulence are also shown in the figure. The dashed (turbine-induced) and dash-dotted (ambient) lines show the variation of each term as a function of radial turbulence intensity obtained from Model ITS (§ 2.4).

in the model for the presented cases in table 1 and the theoretical limits in the extreme of no ambient turbulence are shown in the figure with the symbols. One can observe a considerable increase in the relative contribution of the turbine-induced turbulence by decreasing the turbulence intensity of the incoming ABL flow. In the case with the lowest ambient turbulence (with streamwise turbulence intensity of 0.05), the turbine-induced turbulence contribution to the wake width is around 40 % of the total wake width. To further investigate the relative contribution of the ambient and turbine-induced turbulence to the wake width under a wide range of ambient radial turbulence intensities (from 0 to 0.1), we have used the Model ITS as presented in § 2.4. In that model, the Eulerian integral scale was chosen as the average of those calculated from the five LES cases, as it was found to have a relatively small variability (standard deviation to mean ratio smaller than 0.15). The results are also shown in figure 8 as a dash-dotted line (ambient-turbulence contribution) and a dashed line (turbine-induced contribution). The relative contribution of each term shows a steeper variation with decreasing ambient turbulence intensity. This trend emphasises the importance of the turbine-induced turbulence term of the model for the accurate prediction of the wake growth rate in relatively low ambient turbulence conditions. Further research is required to fill the gap in this region of interest and explore the behaviour of the contributing factors to the wake expansion in the extreme of low turbulence. The importance of the turbine-induced turbulence, along with the limitations of the current empirical formulations for the wake growth rate parameter (a function of the streamwise turbulence intensity alone and valid within a limited range of turbulence intensity levels) supports the importance of having a physics-based model that considers both the effects of ambient turbulence and turbine-induced turbulence.

Figure 9 shows the variation of the near-wake length with the streamwise turbulence intensity calculated from the proposed relations (2.19)–(2.21), and it is compared with that

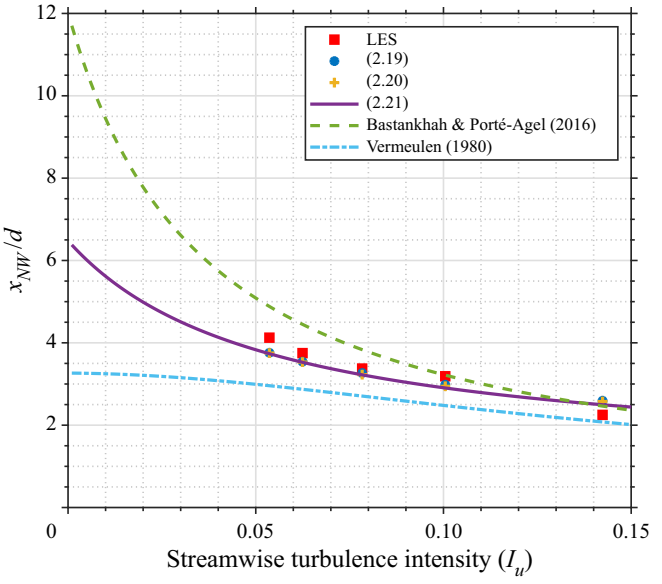

Figure 9. Near-wake length as a function of streamwise turbulence intensity, comparison of the proposed relations (2.19)–(2.21), LES results, the near-wake length proposed by Bastankhah & Porté-Agel (2016) and the near-wake length proposed by Vermeulen (1980).

obtained from the near-wake length model proposed by Bastankhah & Porté-Agel (2016), the near-wake length model proposed by Vermeulen (1980) and LES data. For the LES data, the near-wake length is calculated based on the downstream position where the linear correlation coefficient of the Gaussian fit to the velocity deficit reaches the threshold of 0.99. For the proposed relations in § 2.3, the value of the parameters are the same as those mentioned earlier ($Sc_t = 0.5$, $S' = 0.043$, $x_0/d = 1$, $\sigma_e/d = 0.18$) without any parameter tuning. The other models are used with their original set of parameters. As shown in this figure, the near-wake length increases with decreasing ambient turbulence level. Equations (2.19)–(2.21) capture this behaviour and provide an acceptable prediction of the near-wake length in a wide range of ambient turbulence levels. It should be mentioned that (2.20) is a simplified form of (2.19) based on removing the filtering from the equivalent radial velocity component and (2.21) is strictly valid for neutral atmospheric conditions. Thus, the use of each of the proposed equations should take into account their respective underlying assumptions.

4. Summary and concluding remarks

In this study, a new physics-based model has been proposed to predict the wake growth rate downstream of a wind turbine. The model is based on the Taylor diffusion theory, the Gaussian wake model, turbulent mixing layers self-similarity and the similarity between wind turbine wake expansion and scalar diffusion from a disk source. With these elements in place, the model ensures the conservation of mass and momentum in the far wake and accounts for the effects of both ambient turbulence and turbine-induced turbulence on the total wake width at each downstream location. Moreover, by filtering the velocity time series at each downwind distance, the model takes into account the relevant scales of the incoming turbulence in the wake expansion and removes the high-frequency fluctuations

(small scales). A simplified version of the model has also been derived and only requires as inputs the unfiltered velocity standard deviation and the integral time scales of the radial velocity component of the incoming flow. Another outcome of the proposed modelling framework is a new relation for the near-wake length as a function of the incoming ambient turbulence intensity and turbine operating condition (C_T). In addition, a new functional form for the wake velocity deficit distribution in the near wake has been derived based on a super-Gaussian shape function and a new approach to calculate the smoothness parameter.

The model performance has been validated against LES data of a utility-scale wind turbine wake under neutral ABL conditions with a wide range of incoming ambient turbulence levels. It has been found that the proposed model yields reasonably accurate predictions of the wake width, normalised maximum velocity deficit and near-wake length for all the LES cases. It is particularly noteworthy to mention that the model performs well for low ambient turbulence conditions, for which the existing models are unable to account for the contribution of turbine-induced turbulence on the wake expansion. In summary, the proposed analytical model is found to be simple, fast and reasonably accurate for the prediction of mean turbine wake flows under a wide range of atmospheric turbulence conditions.

Future research will focus on extending the proposed analytical model to calculate the wake velocity deficit distribution inside wind farms with different layout configurations. Moreover, the analytical modelling framework presented in this study should be further tested and, if needed, improved to capture the effect of thermal stability on wind turbine wakes.

Acknowledgements. Computing resources were provided by EPFL through the use of the facilities of its Scientific IT and Application Support Center (SCITAS) and by the Swiss National Super-computing Centre (CSCS).

Funding. This research was funded by the Swiss National Science Foundation (Grant Number 200021_172538) and the Swiss Federal Office of Energy (Grant Number SI/502135-01).

Declaration of interests. The authors report no conflict of interest.

Author ORCIDs.
Dara Vahidi https://orcid.org/0000-0003-1302-9366;
Fernando Porté-Agel https://orcid.org/0000-0002-9913-3350.

Author contributions. Conceptualisation, D.V. and F.P.-A.; data curation, D.V.; formal analysis, D.V.; funding acquisition, F.P.-A.; investigation, D.V. and F.P.-A.; methodology, D.V. and F.P.-A.; project administration, F.P.-A.; resources, F.P.-A.; software, D.V.; supervision, F.P.-A.; validation, D.V.; visualisation, D.V.; writing–original draft, D.V.; writing–review and editing, D.V. and F.P.-A. Both authors have read and agreed to the published version of the manuscript.

Appendix A. Summary of the model

This section provides a concise summary of the model to facilitate its application by the reader. For this purpose, we review the model inputs, the model outputs and the procedure to calculate the outputs of the model, as well as the key variables.

A.1. *Inputs of the model*

The inputs to the model are as follows.

(1) Wind turbine thrust coefficient (C_T).

(2) For the model presented in § 2.2 (Model Filter), the velocity time series sampled upstream of the turbine at hub height, representing the incoming flow conditions in the streamwise, lateral and vertical directions. For the simplified model presented in § 2.4 (Model ITS), the streamwise, lateral and vertical incoming turbulence intensities and the lateral and vertical integral time scales.
(3) The mean incoming wind speed (U_∞).

The parameters of the model are listed below. The value of each parameter is set based on the presented discussions in § 2, without any parameter tuning.

(1) Turbulent Schmidt number, $Sc_t = 0.5$ for mixing layers (Reynolds 1976) (§ 2.2).
(2) Mixing layer characteristic length spreading rate, $S' = 0.043$ (§ 2.1.2).
(3) End of the expansion region, $x_0 = 1d$ (§ 2.2).
(4) Threshold for the onset of the far wake, $\sigma_{e,NW}/d = 0.18$ (§§ 2.1.3 and 2.3).

A.2. *Outputs of the model*

The outputs of the model are as follows.

(1) Near-wake length (x_{NW}).
(2) Wake width (σ_{wake}).
(3) Maximum wake velocity deficit ($(\Delta U/U_\infty)_{max}$).
(4) Wake velocity deficit distribution.

A.3. *Step-by-step procedure*

This section provides a summary for the wake analytical model presented in §§ 2.2–2.5 to estimate the near-wake length, the wake expansion, the maximum wake velocity deficit and the wake velocity deficit profiles until the desired downwind distance. The model is proposed in two versions: one based on filtering the velocity time series with a moving average filter (denoted as Model Filter and presented in § 2.2), and a simplified form based on the integral time scales of the incoming flow and the unfiltered velocity standard deviations (denoted as Model ITS and described in § 2.4). The procedure to obtain the model outputs given the inputs mentioned above is as follows.

(1) The near-wake length (x_{NW}) is calculated based on the inflow data using (2.19), or the simplified forms, as presented in (2.20) and (2.21), whenever applicable.
(2) For the far wake ($x \geq x_{NW}$), the Gaussian model given by (2.16) is applied. The wake width and wake centreline velocity are computed using the following streamwise-marching iterative procedure:
    (4.1) At each downstream location, the wake centreline velocity (U_{centre}) is initialised with the value of the closest upwind position. For each downstream step, from x_0 to the position of interest, the travel time (T) is computed using (2.14). The wake advection velocity and the shear velocity are computed using the U_{centre}. For the Model Filter, given the travel time, the respective filter size (T/β) can be determined to filter the lateral and vertical velocity time series with the moving average filter.
    (4.2) The lateral mixing layer characteristic length (σ_{ey}) is computed using Model Filter (2.15) or Model ITS (2.27).
    (4.3) The lateral wake width ($\sigma_{wake,y}$) is computed from σ_{ey} using the relation given by (2.8), presented in § 2.1.3.

(4.4) Steps (4.2) and (4.3) are repeated for the vertical direction with the respective properties to calculate the σ_{ez} and $\sigma_{wake,z}$.

(4.5) The total wake width and the total mixing layer characteristic length are calculated as the geometrical mean of the lateral and vertical values.

(4.6) The wake centreline velocity (U_{centre}) is computed based on the total wake width using (2.16) in order to guarantee the conservation of momentum.

(4.7) The wake advection velocity (U_{adv}) is computed, and steps (4.1)–(4.7) are repeated until convergence.

(3) For the near wake ($x \leq x_{NW}$), the super-Gaussian model given by (2.28), (2.31) and (2.32) is applied. Note that the model is defined in such a way that it smoothly converges to the aforementioned Gaussian solution at the onset of the far wake.

A.4. *Key variables*

The following is a list of the key variables used in the proposed physics-based analytical modelling procedure.

Sc_t	Turbulent Schmidt number.
σ_y^2	The mean square of the lateral distribution of a large number of particles behind a point source. In this paper, σ_y^2 is used within the formulations of the Taylor diffusion theory, explicitly § 2.1.1 and (2.23) and (2.24).
T_L	Lagrangian integral time scale.
T_E	Eulerian integral time scale.
T_{Lv}	Lagrangian integral time scale for the lateral (v) velocity component.
σ_e	Mixing layer characteristic length.
σ_{wake}	Gaussian wake width.
σ_{ey}	Mixing layer characteristic length in the lateral (y) direction.
$\sigma_{wake,y}$	Gaussian wake width in the lateral direction.
σ_{ez}	Mixing layer characteristic length in the vertical (z) direction.
$\sigma_{wake,z}$	Gaussian wake width in the vertical direction.
S'	The spreading rate for the mixing layer characteristic length (σ_e) defined in § 2.1.2.
d	Wind turbine rotor diameter.
x_{NW}	Near-wake length.
$\sigma_{e,NW}$	Mixing layer characteristic length at the end of the near wake, as a criterion for the onset of the far wake. The value is estimated based on the analogy between the wind turbine wake expansion and the scalar diffusion from a continuous disk source, §§ 2.1.3 and 2.3.
x_0	End of the expansion region.
T	Travel time, (2.14).
U_{centre}	Wake centreline velocity.
ΔU_{max}	Wake shear velocity, defined as $U_\infty - U_{centre}(x)$.
U_{adv}	Wake advection velocity, defined as $U_{adv}(x) = 0.5(U_{centre}(x) + U_\infty)$.
C'	Wake maximum velocity deficit.
n	The super-Gaussian smoothness parameter.
A	The tunable coefficient of the smoothness parameter, defines the super-Gaussian shape at the end of expansion region.
σ'	The super-Gaussian wake width.

References

Abkar, M. & Porté-Agel, F. 2015 Influence of atmospheric stability on wind-turbine wakes: a large-eddy simulation study. *Phys. Fluids* **27** (3), 035104.

Abkar, M., Sørensen, J.N. & Porté-Agel, F. 2018 An analytical model for the effect of vertical wind veer on wind turbine wakes. *Energies* **11** (7), 1838.

Ainslie, J.F. 1988 Calculating the flowfield in the wake of wind turbines. *J. Wind Engng Ind. Aerodyn.* **27** (1–3), 213–224.

Barthelmie, R.J., *et al.* 2009 Modelling and measuring flow and wind turbine wakes in large wind farms offshore. *Wind Energy* **12** (5), 431–444.

Bastankhah, M. & Porté-Agel, F. 2014 A new analytical model for wind-turbine wakes. *Renew. Energy* **70**, 116–123.

Bastankhah, M. & Porté-Agel, F. 2016 Experimental and theoretical study of wind turbine wakes in yawed conditions. *J. Fluid Mech.* **806**, 506–541.

Blondel, F. & Cathelain, M. 2020 An alternative form of the super-Gaussian wind turbine wake model. *Wind Energy Sci.* **5** (3), 1225–1236.

Brown, G.L. & Roshko, A. 1974 On density effects and large structure in turbulent mixing layers. *J. Fluid Mech.* **64** (4), 775–816.

Brugger, P., Fuertes, F.C., Vahidzadeh, M., Markfort, C.D. & Porté-Agel, F. 2019 Characterization of wind turbine wakes with nacelle-mounted doppler lidars and model validation in the presence of wind veer. *Remote Sens.* **11** (19), 2247.

Carbajo Fuertes, F., Markfort, C.D. & Porté-Agel, F. 2018 Wind turbine wake characterization with nacelle-mounted wind lidars for analytical wake model validation. *Remote Sens.* **10** (5), 668.

Chamorro, L.P. & Porté-Agel, F. 2009 A wind-tunnel investigation of wind-turbine wakes: boundary-layer turbulence effects. *Boundary-Layer Meteorol.* **132** (1), 129–149.

Cheng, W.C. & Porté-Agel, F. 2018 A simple physically-based model for wind-turbine wake growth in a turbulent boundary layer. *Boundary-Layer Meteorol.* **169** (1), 1–10.

Crank, J. 1979 *The Mathematics of Diffusion*. Oxford University Press.

Crespo, A., Hernandez, J. & Frandsen, S. 1999 Survey of modelling methods for wind turbine wakes and wind farms. *Wind Energy: Intl J. Prog. Appl. Wind Power Convers. Technol.* **2** (1), 1–24.

Dimotakis, P.E. 1986 Two-dimensional shear-layer entrainment. *AIAA J.* **24** (11), 1791–1796.

Duckworth, A. & Barthelmie, R.J. 2008 Investigation and validation of wind turbine wake models. *Wind Engng* **32** (5), 459–475.

Eames, I., Jonsson, C. & Johnson, P.B. 2011*b* The growth of a cylinder wake in turbulent flow. *J. Turbul.* **12**, N39.

Eames, I., Johnson, P.B., Roig, V. & Risso, F. 2011 Effect of turbulence on the downstream velocity deficit of a rigid sphere. *Phys. Fluids* **23** (9), 095103.

Edenhofer, O., *et al.* (Eds.) 2011 *Renewable Energy Sources and Climate Change Mitigation: Special Report of the Intergovernmental Panel on Climate Change*. Cambridge University Press.

Frandsen, S. 2007 *Turbulence and Turbulence-Generated Structural Loading in Wind Turbine Clusters*. PhD thesis, Risø National Laboratory.

Frandsen, S., Barthelmie, R., Pryor, S., Rathmann, O., Larsen, S., Højstrup, J. & Thøgersen, M. 2006 Analytical modelling of wind speed deficit in large offshore wind farms. *Wind Energy: Intl J. Prog. Appl. Wind Power Convers. Technol.* **9** (1–2), 39–53.

Gifford, F. 1955 A simultaneous Lagrangian–Eulerian turbulence experiment. *Mon. Weath. Rev.* **83**, 293–301.

Göçmen, T., Van der Laan, P., Réthoré, P.E., Diaz, A.P., Larsen, G.C. & Ott, S.T. 2016 Wind turbine wake models developed at the Technical University of Denmark: a review. *Renew. Sustain. Energy Rev.* **60**, 752–769.

Hanna, S.R. 1981 Lagrangian and Eulerian time-scale relations in the daytime boundary layer. *J. Appl. Meteorol.* **20** (3), 242–249.

Hanna, S.R., Briggs, G.A. & Hosker, R.P. Jr. 1982 Handbook on atmospheric diffusion. *Tech. Rep.*. National Oceanic and Atmospheric Administration.

Hansen, M. 2015 *Aerodynamics of Wind Turbines*. Routledge.

Hay, J.S. & Pasquill, F. 1959 Diffusion from a continuous source in relation to the spectrum and scale of turbulence. In *Advances in Geophysics*, vol. 6, pp. 345–365. Elsevier.

Howland, M.F., Ghate, A.S, Lele, S.K. & Dabiri, J.O. 2020 Optimal closed-loop wake steering–part 1: conventionally neutral atmospheric boundary layer conditions. *Wind Energy Sci.* **5** (4), 1315–1338.

Jensen, N.O. 1983 A note on wind turbine interaction, p. 16. *Riso-M-2411*. Risoe National Laboratory.

KEANE, A. 2021 Advancement of an analytical double-gaussian full wind turbine wake model. *Renew. Energy* **171**, 687–708.

KEANE, A., AGUIRRE, P.E.O., FERCHLAND, H., CLIVE, P. & GALLACHER, D. 2016 An analytical model for a full wind turbine wake. In *Journal of Physics: Conference Series*, vol. 753, p. 032039. IOP Publishing.

KROGSTAD, P.Å. & ADARAMOLA, M.S. 2012 Performance and near wake measurements of a model horizontal axis wind turbine. *Wind Energy* **15** (5), 743–756.

LARSEN, G.C., MADSEN, H.A., THOMSEN, K. & LARSEN, T.J. 2008 Wake meandering: a pragmatic approach. *Wind Energy: Intl J. Prog. Appl. Wind Power Convers. Technol.* **11** (4), 377–395.

LISSAMAN, P.B.S. 1979 Energy effectiveness of arbitrary arrays of wind turbines. *J. Energy* **3** (6), 323–328.

MIKKELSEN, R. 2003 Actuator disc methods applied to wind turbines. PhD thesis, Technical University of Denmark.

NEUMANN, J. 1978 Some observations on the simple exponential function as a Lagrangian velocity correlation function in turbulent diffusion. *Atmos. Environ.* **12** (10), 1965–1968.

NIAYIFAR, A. & PORTÉ-AGEL, F. 2016 Analytical modeling of wind farms: a new approach for power prediction. *Energies* **9** (9), 741.

PANOFSKY, H.A. 1984 Atmospheric Turbulence: Models and Methods for Engineering Applications. Wiley-Blackwell.

PASQUILL, F. & SMITH, F.B. 1983 *Atmospheric Diffusion*, vol. 437. Ellis Horwood.

POPE, S.B. 2000 *Turbulent Flows*. Cambridge University Press.

PORTÉ-AGEL, F., BASTANKHAH, M. & SHAMSODDIN, S. 2020 Wind-turbine and wind-farm flows: a review. *Boundary-Layer Meteorol.* **174** (1), 1–59.

PORTÉ-AGEL, F., WU, Y.T. & CHEN, C.H. 2013 A numerical study of the effects of wind direction on turbine wakes and power losses in a large wind farm. *Energies* **6** (10), 5297–5313.

PORTÉ-AGEL, F., WU, Y.T., LU, H. & CONZEMIUS, R.J. 2011 Large-eddy simulation of atmospheric boundary layer flow through wind turbines and wind farms. *J. Wind Engng Ind. Aerodyn.* **99** (4), 154–168.

REVAZ, T. & PORTÉ-AGEL, F. 2021 Large-eddy simulation of wind turbine flows: a new evaluation of actuator disk models. *Energies* **14** (13), 3745.

REYNOLDS, A.J. 1976 The variation of turbulent Prandtl and Schmidt numbers in wakes and jets. *Intl J. Heat Mass Transfer* **19** (7), 757–764.

SANDERSE, B., VAN DER PIJL, S.P. & KOREN, B. 2011 Review of computational fluid dynamics for wind turbine wake aerodynamics. *Wind Energy* **14** (7), 799–819.

SCHREIBER, J., BALBAA, A. & BOTTASSO, C.L. 2020*a* Brief communication: a double-Gaussian wake model. *Wind Energy Sci.* **5** (1), 237–244.

SCHREIBER, J., BOTTASSO, C.L., SALBERT, B. & CAMPAGNOLO, F. 2020*b* Improving wind farm flow models by learning from operational data. *Wind Energy Sci.* **5** (2), 647–673.

SHAPIRO, C.R., STARKE, G.M., MENEVEAU, C. & GAYME, D.F. 2019 A wake modeling paradigm for wind farm design and control. *Energies* **12** (15), 2956.

SØRENSEN, J.N., MIKKELSEN, R.F., HENNINGSON, D.S., IVANELL, S., SARMAST, S. & ANDERSEN, S.J. 2015 Simulation of wind turbine wakes using the actuator line technique. *Phil. Trans. R. Soc. A: Math. Phys. Engng Sci.* **373** (2035), 20140071.

STEVENS, R.J. & MENEVEAU, C. 2017 Flow structure and turbulence in wind farms. *Annu. Rev. Fluid Mech.* **49**, 311–339.

STOLL, R. & PORTÉ-AGEL, F. 2006 Dynamic subgrid-scale models for momentum and scalar fluxes in large-eddy simulations of neutrally stratified atmospheric boundary layers over heterogeneous terrain. *Water Resour. Res.* **42** (1), W01409.

TAYLOR, G.I. 1922 Diffusion by continuous movements. *Proc. Lond. Math. Soc.* **2** (1), 196–212.

TENG, J. & MARKFORT, C.D. 2020 A calibration procedure for an analytical wake model using wind farm operational data. *Energies* **13** (14), 3537.

TENNEKES, H. & LUMLEY, J.L. 1972 *A First Course in Turbulence*. MIT Press.

VERMEULEN, P.E.J. 1980 An experimental analysis of wind turbine wakes. In *3rd International Symposium on Wind Energy Systems, Lyngby, Denmark*, pp. 431–450.

WU, Y.T. & PORTÉ-AGEL, F. 2011 Large-eddy simulation of wind-turbine wakes: evaluation of turbine parametrisations. *Boundary-Layer Meteorol.* **138** (3), 345–366.

WU, Y.T. & PORTÉ-AGEL, F. 2012 Atmospheric turbulence effects on wind-turbine wakes: an LES study. *Energies* **5** (12), 5340–5362.

XIE, S. & ARCHER, C. 2015 Self-similarity and turbulence characteristics of wind turbine wakes via large-eddy simulation. *Wind Energy* **18** (10), 1815–1838.

ZONG, H. & PORTÉ-AGEL, F. 2020 A momentum-conserving wake superposition method for wind farm power prediction. *J. Fluid Mech.* **889**.